Pergamon

Int. J. Solids Structures Vol. 35, No. 33, pp. 4411–4426, 1998

0020–7683/98 $19.00 + .00

PII: S0020–7683(97)00249–7

NEW ANALYTICAL PROCEDURE TO DETERMINE STRESS–STRAIN CURVE FROM SPHERICAL INDENTATION DATA

B. TALJAT, T. ZACHARIA
Oak Ridge National Laboratory, Metals and Ceramics Division, Oak Ridge, TN 37831-6140, U.S.A.

and

F. KOSEL
University of Ljubljana, Faculty of Mechanical Engineering, Askerceva 6, 1000 Ljubljana, Slovenia

(*Received* 12 *November* 1996; *in revised form* 6 *August* 1997)

Abstract—Spherical-indentation process was analyzed by finite element (FE) method. A systematic analysis of relationship between indentation parameters and true stress/plastic–strain (σ_t–ε_p) curve was performed for a range of material properties. An existing method relates the ratio or residual contact diameter, d, and indenter diameter, D, to ε_p by the well-known Tabor's empirical equation $\varepsilon_p = 0.2d/D$. The method is based on parameters of residual indentation, where a loading-unloading cycle needs to be made in order to calculate a point on σ_t–ε_p curve. A new analytical approach is presented which relates the indentation data continuously measured during loading to σ_t–ε_p curve. ε_p calculated by the new method is in the range from yield strain to a strain between 0.3 and 1.6, depending on material's strain hardening properties. In addition, different measures of indentation diameter are discussed and their influence on the resulting σ_t–ε_p curve analyzed. Experimental work was performed by an instrumented spherical-indentation technique in order to verify the FE analysis results. A good agreement between the FE and experimental results was obtained. © 1998 Elsevier Science Ltd. All rights reserved.

1. INTRODUCTION

A concept for relating parameters of a spherical indentation to the material true stress/plastic–strain (σ_t–ε_p) curve was introduced by Tabor (1951). He presented an important correlation between ε_p and indentation parameters: $\varepsilon_p = 0.2d/D$, where d is the contact diameter of a residual indentation and D is the indenter diameter. Tabor also found that the corresponding stress value could be determined as one third of the mean pressure beneath the indenter of a fully plastic indentation. Several other authors (Francis, 1976; Johnson, 1970; Sinclair *et al.*, 1985; Au *et al.*, 1980) have also worked on development of relations between σ_t and indentation parameters, always assuming Tabor's ε_p relationship as a basis.

As a result, the spherical-indentation method can today be used as an experimental procedure for obtaining flow properties of metals (Field and Swain, 1995). The spherical-indentation technique is a unique method for determining material stress–strain behaviour in a nondestructive and localized fashion. This is important in measuring local flow properties of welds, heat-affected zones, and metallic structures in operation.

Rapid advances in computational mechanics in the last decade have produced the means to analyze the mechanical components under fully non-linear plastic conditions. As an example, very sophisticated computer codes (ABAQUS, MSC-NASTRAN, DYNA 3D, ANSYS) have been developed that enable numerical modeling of highly non-linear processes such as metal forming. In these applications, ε_p often exceeds the value of 0.2, and therefore the stress–strain relations should also apply to higher strain values. On the other hand, the yield strength provides an important material information, as does the early

* Author to whom correspondence should be addressed.

portion of the stress–strain curve. Improving the data analysis of the spherical indentation in order to accurately predict stress–strain curves at very low strains and to obtain its large strain portion will empower the indentation technique and satisfy the above mentioned requirements.

A finite element (FE) model of a spherical indentation process was developed. The analysis was performed using ABAQUS (1996) computer code. Several simulations were performed analyzing the response of the stress–strain field beneath the indenter and the response of the load-depth curve to variations in different material properties. On the basis of the FE results, a new set of equations relating the material flow properties to the indentation parameters was developed. The advantage of the developed equations is a significant extension of strain range over which the σ_t–ε_p curve can be determined. Also, a continuous σ_t–ε_p curve is calculated during loading of the indenter, in contrast to the old approach, where an unloading is required to determine a point on the σ_t–ε_p curve. Different indentation diameter measures were considered and their influence on the calculated σ_t–ε_p curve was analyzed. The significance of having the right measure of the indentation diameter was emphasized.

Experimental compression and indentation testing was performed on five materials with different mechanical properties (A533-B steel, SAE1010 steel, Al–Mg alloy, annealed copper, and cold-worked copper). Compression tests were conducted to measure the uniaxial σ_t–ε_p curves, which were used as an input to the FE analyses. Indentation experiments were performed to verify the FE results.

2. OVERVIEW OF THEORY

True-stress is correlated to the mean pressure underneath the indenter, P_m, which is the ratio between the applied force, F, and the projected indentation area, $\pi d^2/4$ (Tabor, 1951):

$$\sigma_t = \frac{P_m}{\psi}. \tag{1}$$

The parameter ψ is called the constraint factor and is, according to Francis (1976), represented as a function of the parameter Φ:

$$\psi = \begin{cases} C_1 & \Phi \leqslant 1 \\ C_1 + C_2 \ln\Phi & 1 < \Phi \leqslant C_3, \\ \psi^c & \Phi > C_3 \end{cases} \tag{2}$$

where

$$\Phi = \tan(\vartheta)\frac{E}{\sigma_t} = \frac{4Eh_{p^s}}{d\sigma_t}. \tag{3a}$$

Equation (2) defines three mechanical stages: elastic, where after load removal the material recovers elastically and ψ has a constant value of 1.11; transition, which is a combination of elastic and plastic deformation and ψ is a linear function of $\ln(\Phi)$; and fully plastic, where the plastic deformation, which initiates in the material beneath the indenter reaches the free material surface and ψ has a constant value ψ^c. Different values can be obtained for parameters C_1, C_2, C_3, and ψ^c from the literature (Tabor, 1951; Francis, 1976; Au *et al.*, 1980; Field and Swain, 1995). Since Francis (1976) worked on statistical analysis of previously published experimental data, we may take his computed values for $C_1 = 1.11$, $C_2 = 0.534$, $C_3 = 27.3$, and $\psi^c = 2.87$ as the average values. The parameter ϑ is the angle between the tangent to the indenter at the indentation edge and the original surface. The parameter Φ may be interpreted as a ratio of the strain imposed by the indenter to the

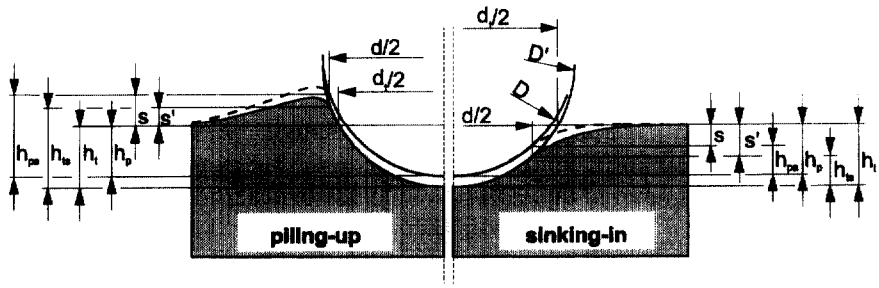

Fig. 1. Schematic of spherical-indentation geometries.

maximum strain which can be accommodated by the material before yielding (Johnson, 1970). For shallow indentations, where $d \ll D$, one can rewrite eqn (3a) as:

$$\Phi = \frac{Ed}{\sigma_t D}. \tag{3b}$$

The parameter Φ for loaded indentations was defined in the current work as:

$$\Phi = \frac{4Eh_t}{d_t\sigma_t}, \tag{3c}$$

where E is Young's modulus of material, parameters h_t and h_{ps} are defined in Fig. 1, and the parameter d_t is defined in eqn (8). Figure 1 is a schematic of the indentation cross-section illustrating the main indentation parameters. Typical materials, where piling-up appears include cold-worked materials. Sinking-in effects, on the other hand, are typical for annealed materials.

Tabor (1951) defined the relationship between true-plastic strain and the indentation parameter d/D as:

$$\varepsilon_p = 0.2d/D. \tag{4}$$

The calculated σ_t and ε_p values correspond to stress and strain values at the indentation edge, called also "representative stress and strain" (Tabor, 1951).

Equation (2) does not predict the constraint factor dependency on the strain hardening exponent, n, defined by equation: $\sigma_t = K\varepsilon_p^n$, where K is the strength coefficient. However, the results of Matthews (1980) and Tirupataiah (1991) demonstrate such dependency. Matthews has also presented an approximate equation for the mean contact pressure for a work-hardening material from which ψ^c can be written as a function of n:

$$\psi^c = \frac{P_m}{\sigma_t} = \frac{6}{2+n}\left(\frac{40}{9\pi}\right)^n. \tag{5}$$

Equation (5) gives the value $\psi^c = 3$ for $n = 0$, and $\psi^c = 2.85$ for $n = 0.5$. The experimental results of Tirupataiah show the same trend: higher ψ^c at lower n and vice versa. His measured ψ^c values vary between 2.4 and 3.1 for different materials.

Method presented by Au *et al.* (1980) uses the indentation diameter, d', calculated by Hertz's equation (Hertz, 1896):

$$d' = \left(\frac{3FD}{E_r}\,\frac{h_p^2+(d'/2)^2}{h_p^2+(d'/2)^2-h_pD}\right)^{1/3}, \tag{6}$$

where

$$\frac{1}{E_r} = \frac{1-\nu_I^2}{E_I} + \frac{1-\nu^2}{E}. \tag{7}$$

E is elastic modulus and ν is Poissons's ratio for the material (E, ν) and the indenter (E_I, ν_I), h_p is the plastic indentation depth, and h_t is the total indentation depth (see Fig. 1). Several progressive loadings and unloadings were made in order to provide h_p data, which is necessary to calculate d' (Au *et al.*, 1980). According to Tabor (1951), eqn (6) gives good results for shallow indentations, but a large discrepancy appears for deeper indentations. Also, according to the results of our FE calculations, the results obtained by eqn (6) are almost identical (average difference is about 1% over the range of $0.1 \leqslant d/D \leqslant 0.7$ for an $E/\sigma_y = 500$ material where σ_y is the yield stress) to the indentation for diameter, d_t, calculated as a diameter of the intersection between the indenter and the original material surface under loading (see Fig. 1):

$$d_t = 2\sqrt{h_t(D-h_t)}. \tag{8}$$

This is because eqn (6) was developed with the assumption of an ideal spherical depression in which the diameter before and after load application is the same. This means that d as calculated by eqn (6) is essentially identical to d_t, if one neglects the change of indentation diameter caused by the indenter's elastic deformation. This also means that neither eqn (6) nor eqn (8) accounts for changes in the indentation diameter due to the piling-up or sinking-in effect, which turns out to be very important for measuring the appropriate contact surface. The importance of this effect was shown by Norbury and Samuel (1928), and emphasized later by Hill *et al.* (1989) and Field and Swain (1995).

According to Norbury and Samuel (1928), raising (piling-up) or depressing the circle of contact (sinking-in) relative to the original surface correlates with n (see Fig. 5). They measured the contact diameter on recovered indentations and calculated its relative height to the original surface. The result of their research is a relationship between the ratio of s/h_p and m, where s represents the height/depth of the pile-up/sink-in from the original surface ($s = h_{ps} - h_p$), m is the Meyer's index represented as $F = kd^m$, and k is a material parameter. Furthermore, it was observed that the expression $n = m-2$ is valid for a broad range of materials (see Tabor, 1951). Hill *et al.* (1989) called the ratio h_{ps}/h_p a numerical invariant c^2, which depends on n. From the geometry of a loaded shallow indentation follows that h_{ts} and h_t can be approximated by $d^2/4D$ and $d_t^2/4D$ respectively, which allows the invariant c^2 to be expressed as:

$$c^2 = \frac{h_{ps}}{h_p} \cong \frac{h_{ts}}{h_t} \text{ and } \cong \frac{d^2}{d_t^2} \text{ (when } d \ll D\text{)}. \tag{9}$$

Different authors expressed it with different equations. Matthews (1980) proposed the following equation as a fit to the Norbury c^2 vs n data:

$$c^2 = \frac{1}{2}\left(\frac{2+n}{2}\right)^{\frac{2(1-n)}{n}}. \tag{10}$$

The following equation, determined by FE computations using a nonlinear elastic constitutive model, was proposed by Hill *et al.* (1989):

$$c^2 = \frac{5}{2}\left(\frac{2-n}{4+n}\right). \tag{11}$$

In order to calculate d using above equations, a measure of h_p is required, as when one calculates d' by eqn (6). The difference between the two approaches is that eqn (9), together

with supportive eqn (10) or (11), represents an empirical approach, that tends to predict the actual indentation diameter by accounting for the piling-up or sinking-in effect, in contrast to eqn (6), which is an analytical solution of the contact problem and deals with an ideal indentation shape.

3. FE ANALYSIS OF THE INDENTATION PROCESS

Elastic-plastic simulation of the indentation process was performed by ABAQUS (1996) FE code. Different axisymmetric FE models were developed to study the effect of

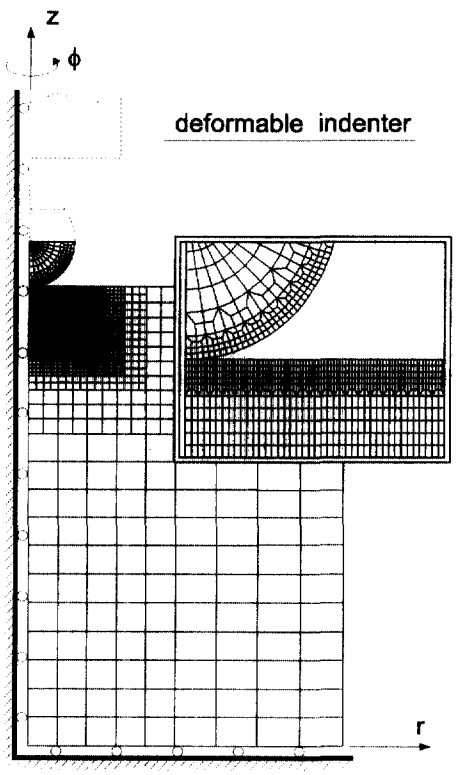

(a)

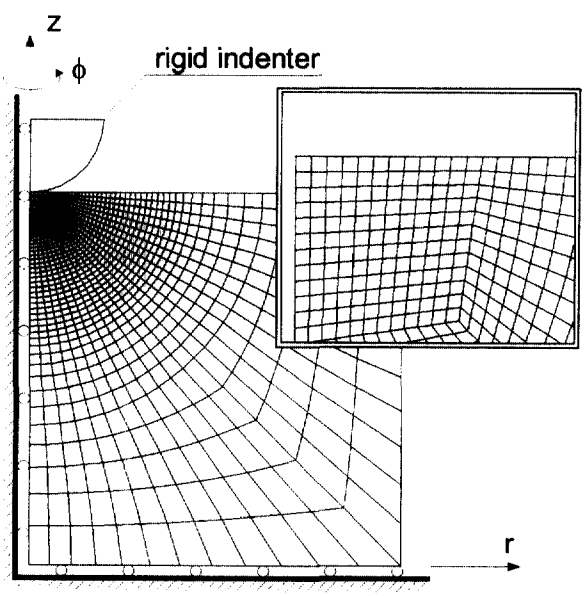

(b)

Fig. 2. Finite element models.

mesh shape and density, element type, and contact definition on the indentation load-depth (F–h) results. The indenter diameter used in the analysis was in the range from 1.576 to 40 mm, dependent on the indentation depth analyzed. The indenter diameter of 1.576 mm was used for model verification, matching the indenter diameter of the experimental system. The cylindrical specimen of 8 mm in diameter and 8 mm in height was modeled by 1571 linear four-node elements and used in the majority of calculations (see Fig. 2a). Two other models were developed to determine the modeling effects on the F–h results. A specimen of 8 mm in diameter and 4 mm in height was modeled by 588 linear four-node elements and by quadratic eight-node elements (see Fig. 2b). For indentations made with larger indenters a specimen of 30 mm in diameter and 20 mm in height, meshed by a similar, but expanded mesh to that in Fig. 2a was used. A cylindrical coordinate system with radial coordinate, r, and axial coordinate, z, was used in all models. As shown in Fig. 2, the bottom surface of the specimen has the z displacement fixed, whereas a free movement was allowed in the r direction. The appropriate boundary conditions to model the axisymmetric behavior were applied along the centerline, and a free surface was modeled at the top and outside surface of the specimen. The influence of friction at the interface between the indenter and the specimen on the F-h curve was evaluated by varying the friction coefficient between 0.0 and 1.0. The friction coefficient of 0.2 was used in the verification analyses and in the analyses that supported the new method development.

The elastic-plastic constitutive behavior was assumed for the materials used in the study. A constant Young's modulus of 200 GPa and a constant yield stress of 400 MPa was used in development of the new method, resulting in an E/σ_y ratio of 500. However, by using the appropriate non-dimensionalization the computed results can be generalized for materials with different E and σ_y. The plastic constitutive behavior was represented by $\sigma_t = K\varepsilon_p^n$ power law curves and the Von Mises yield criterion was assumed. A set of uniaxial true stress/plastic–strain (σ_t–ε_p) curves was defined by varying the strain hardening exponent, n, in the range from 0.0 (elastic/ideal-plastic material) to 0.5. The strength coefficient, K, for each of these curves was calculated with the assumption that the power law constitutive behavior starts at the point defined by a 0.002 offset of the yield strain. According to this assumption K was calculated as $K = \sigma_y/(\sigma_y/E+0.002)^n$. The Poisson's ratio of 0.3 was used in all analyses. An elastic material with E = 645 GPa and a Poisson's ratio of 0.28 was used for the deformable indenter.

As a part of the new procedure development the effect of material properties on the F–h data was studied. The unloading part of the F–h curve is primarily influenced by E, as the unloading process is essentially an elastic process; also shown by Taljat *et al.* (1997). They also showed that the loading part of the F–h curve correlates with σ_y and n. Due to the fact that the computed indentation F–h data can be generalized by an appropriate normalization to account for different σ_y and E, the effect of parameter n was of primary interest in this study. It was assumed that the results obtained for an E/σ_y = 500 material adequately represent indentation deformation behavior of basic engineering metals, limited by Al-Mg alloy at one, and annealed copper at the other end. The behavior of materials with extreme properties may be different (see Bolshkov *et al.*, 1996).

The simulation was essentially used to calculate F–h curves for the defined range of material properties and to analyze the stress–strain distributions in the material, which was used as a basis for development of the new method. The obtained results also gave the possibility to verify the existing equations which relate indentation data to the σ_t–ε_p curve.

3.1. *FE model verification*

Experimental indentation measurements for verification purposes were performed on three different materials: A533-B steel, Al–Mg alloy, and cold-worked copper. An instrumented indentation system was used to perform the measurements. The details of the system are explained in the following section and elsewhere (Taljat, 1996). Also, compression tests were performed on the same materials to determine the σ_t–ε_p curves used as an input in the FE analyses. The compression curves are presented in Fig. 11. Elastic moduli of 210 GPa, 117 GPa, and 70 GPa were used for A533-B steel, cold-worked copper, and

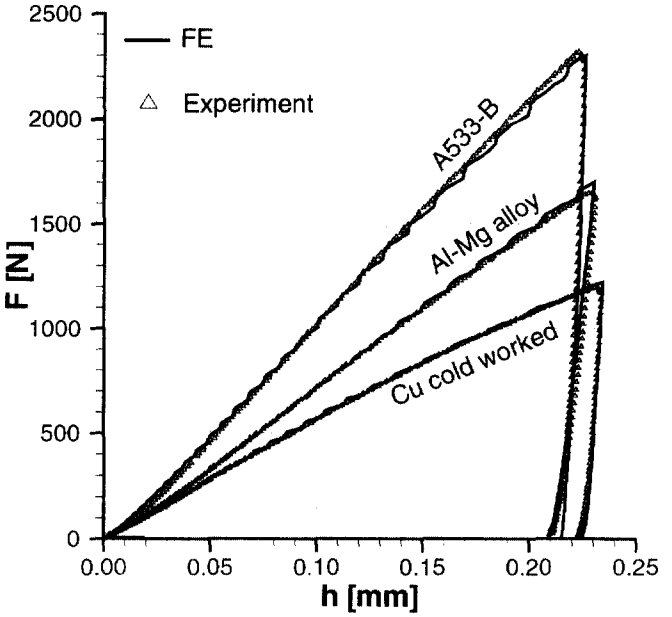

Fig. 3. Comparison between finite element and experimental results.

Al–Mg alloy respectively. Poisson's ratio of 0.3 was used in all three cases. Fig. 3 shows a comparison between the FE and experimental F–h results.

The effects of mesh density, mesh shape, element type, type of indenter model, and contact definitions on the analysis results were investigated. The evaluation of various effects was based on the computed F–h data. FE model verification provided the following information:

1. A very small influence of different mesh shapes and element types on the analysis results was found. Good results were obtained with a mesh density of about 100 elements in contact with the indenter. Reducing the number of elements beneath the indenter to 50 slightly affected the F–h result.
2. The friction coefficient at the indenter-material contact was varied from 0.0 to 1.0. The influence on the F–h results was negligible when the friction coefficient equal or higher than 0.2 was used, but an effect on the stress–strain distribution beneath the indenter was observed. A large difference in the computed F–h data was obtained when a frictionless contact or very low friction coefficients (<0.05) were assumed.
3. The indenter was modeled as a rigid and a deformable body. The penetration depth of a node in contact at the indentation center was computed for both indenter types. In comparing the penetration depth results a negligible difference was detected. On the other hand, a large difference was detected when the calculated results were compared with experimental results. It was proved that the difference is due to the indenter compliance (Taljat *et al.*, 1997), which cannot be ignored, even though the indenter's elastic modulus is at least three times higher than the elastic modulus of the materials. Indenter compliance was taken into account by modeling the indenter up to the point where the depth sensor is mounted. Comparison of the experimentally measured and calculated F–h results at this point shows a very good agreement (see Fig. 3). All the subsequent indentation depth results are evaluated at the indenter-material contact, because it represents the actual material behavior.

3.2. *Calculating indentation diameter*

The FE analysis results showed a large piling-up or sinking-in effect which affects the calculation of indentation diameter. The calculated profiles were compared to the

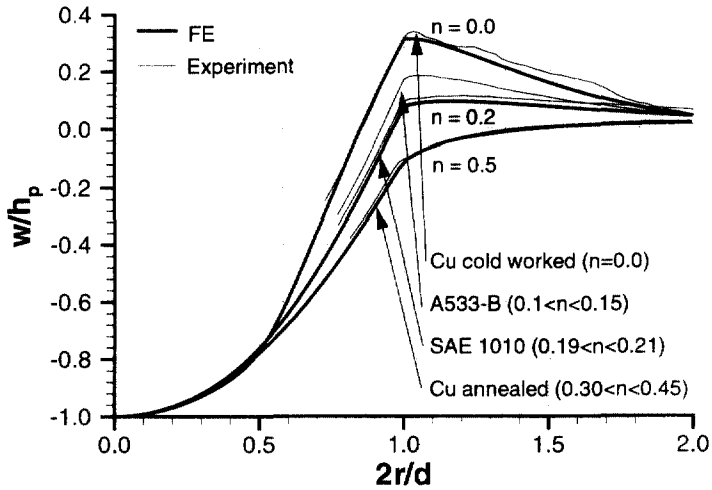

Fig. 4. Indentation profile as a function of n (piling-up and sinking-in effect). Comparison between FE and experiment. $w = z -$ (specimen height).

experimentally measured profiles for different materials and a good agreement was obtained (see Fig. 4).

Figure 5 shows the experimental c^2 vs n data of the current work, the data measured by Norbury and Samuel (1928), and the FE data of loaded and unloaded indentations computed for an $E/\sigma_y = 500$ material. A good comparison with the data of Norbury and Samuel (1928) was obtained. Different c^2 data for loaded and unloaded indentations are due to elastic recovery, which considerably affects the indentation depth and so the calculated d_t, whereas the change in actual contact diameter, d, during unloading is not significant (up to 2% for materials that exhibit sink-in; the change is even smaller for other materials; calculated for $d/D < 0.75$). The results show that the pile-up and sink-in effect depends on n. An $E/\sigma_y = 500$ material shows the pile-up behavior at low n ($n < 0.2$) and sink-in behavior at higher n ($n > 0.2$). The FE results at Fig. 5 are reported at $d/D = 0.5$.

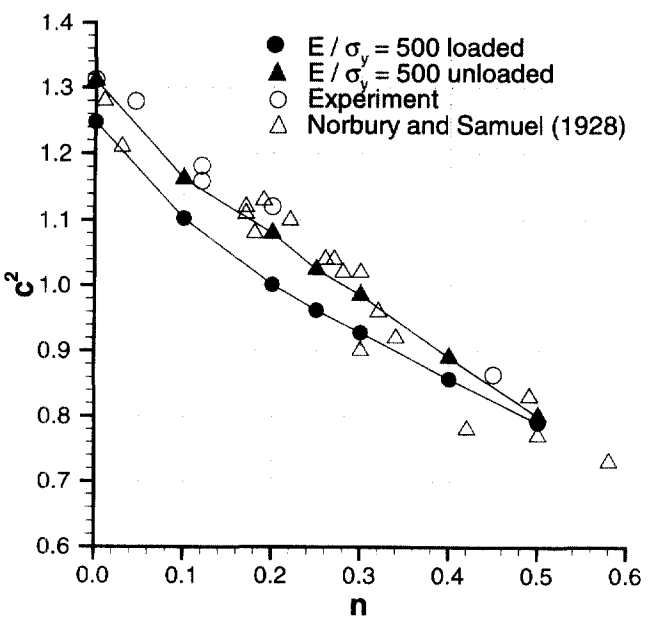

Fig. 5. Quantitative representation of the piling-up and sinking-in effect as a function of n.

The functional relationships between n and c^2, based on the computed FE data for an $E/\sigma_y = 500$ material of loaded (c_l) and unloaded indentations (c), can be represented by:

$$\text{loaded: } c_l^2 = \frac{h_{ts}}{h_t} = \frac{1}{4}(5-3n^{7/10}), \quad \text{unloaded: } c^2 = \frac{1}{10}(13-8.5n^{8/10}). \tag{12}$$

One can use the invariant c to calculate the actual diameter d from the measured d_t using eqn (9) only for shallow indentations ($d \ll D$) under loading. In some cases the equation may give good results for deeper loaded indentations, whereas caution should be exercised for unloaded indentations. A significant elastic recovery in some elastic-plastic materials causes higher curvature of the residual indentation, which may cause large discrepancies in the calculated values of d_t and d.

3.3. *Stress–strain curve calculation*

3.3.1. *Tabor's approach.* Tabor chose stress and strain values at the indentation edge as the representative values for the whole of the deformed material around the impression (Tabor, 1951). These values were then related to the indentation parameters by the empirical equations discussed in Sect. II. Tabor's equation [see eqn (4)] enables the calculation of ε_p up to a value of 0.2.

The approach seems to be easily verified with the FE analysis results when the actual contact diameter, d, is taken into account. The indentation F–d data computed for materials with n in the range from 0.0 to 0.5 were used to produce the ψ–Φ plot. In this case σ_t was defined as the representative indentation flow stress and was calculated using the constitutive σ_t–ε_p relationship, defining the input to the FE code, combined with eqn (4). A fairly good agreement was obtained with ψ–Φ results presented by Francis (1976) and Johnson (1970). As shown in Fig. 6, the calculated value of ψ^c is equal to three for an elastic-ideal-plastic material, and decrease below three for materials with higher n. This agrees very well with the results presented by Matthews (1980) and Tirupataiah (1991).

The FE analysis results give some other possibilities for verifying the empirical equations presented in Sec. II:

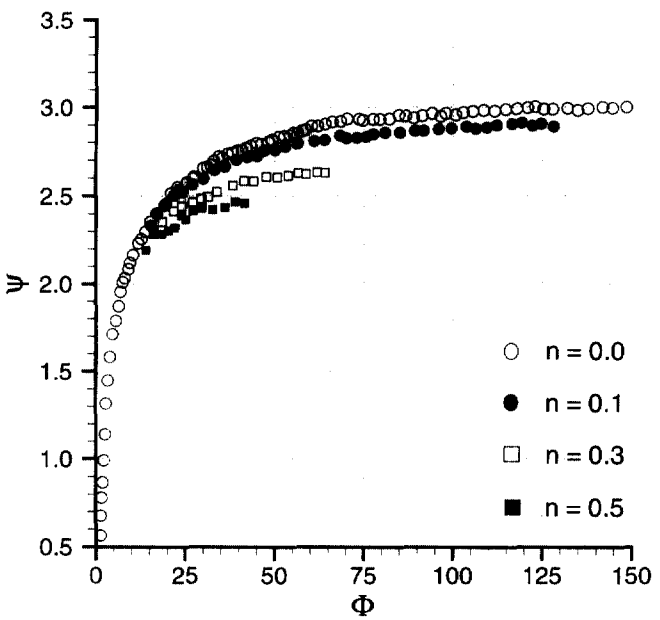

Fig. 6. Constraint factor calculated for the representative stress and strain values at the indentation edge.

1. By applying the empirical equations to the calculated F–h data the σ_r–ε_p curve can be calculated, which should be equal to the input σ_r–ε_p curve to the FE analysis.
2. Tabor's equation [see eqn (4)] can also be verified by the calculated strain distribution in the material. This has already been done by Hill *et al.* (1989) and by Sinclair *et al.* (1985). They compared octahedral strain at the "representative point" calculated by their FE code to ε_p calculated by eqn (4).

A similar comparison was made here. Using the FE method, the equivalent plastic strain, ε_{eq}^{pl}, was calculated at the indentation edge for an $E/\sigma_y = 500$ material with three different strain hardening exponents, $n = 0.0$, 0.25, and 0.5, and the results were compared to ε_p calculated by eqn (4). The values of ε_{eq}^{pl} were computed at $d/D = 0.5$, which gives the value of ε_p equal to 0.1. The computed values of ε_{eq}^{pl} at the indentation edge are within 0.05 and 0.15. The gradient of ε_{eq}^{pl} at the indentation edge is very high, which contributes to the discrepancy in results evaluated exactly at the indentation edge. The ε_{eq}^{pl} curves for all three cases intersect the value of 0.1 in the region from $0.97d$ to $1.03d$, which can be considered a good agreement (see Fig. 7).

If one applies the indentation diameter calculated by eqns (8) or (6) to eqn (1) and calculates parameters ψ and Φ, a common transition curve in the ψ–Φ plot is obtained for materials with different n. A large variety in the ψ^c values for the fully plastic regime is shown on the same plot (see Fig. 8). Materials with low n show a high ψ^c value, and vice versa. In this case ψ accounts for two effects of n: (1) a direct effect, as shown before (see Fig. 6), when the actual indentation diameter was used (also shown by Matthews, 1980; Tipataiah, 1991); and (2) an indirect effect, as a parameter governing piling-up and sinking-in, which actually affects the indentation diameter. The indirect effect of n is in this case more pronounced, since the ψ^c values are in the range from about 1.5 to almost 4.0 for $n = 0.5$ and $n = 0.0$, respectively. This suggests that: (1) it is important to accurately measure or calculate the actual contact diameter when one uses a ψ value around three (approaches by Tabor, 1951; Francis, 1976; Matthews, 1980), or (2) one could calculate the indentation diameter by eqn (8) and use the ψ value which accounts for the difference between d_i and the actual contact diameter; apply ψ as presented in Fig. 8.

3.3.2. *Maximum strain method.*

The FE results show a small value of ε_{eq}^{pl} at the indentation edge, which increases with a high gradient toward the indentation center (see Fig. 7). At a certain distance from the

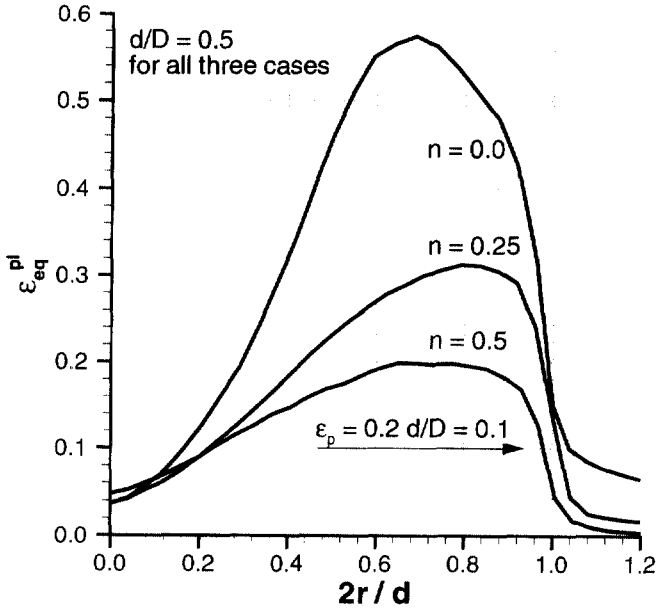

Fig. 7. Equivalent plastic strain at the indentation edge for $n = 0.0$, $n = 0.25$, and $n = 0.5$.

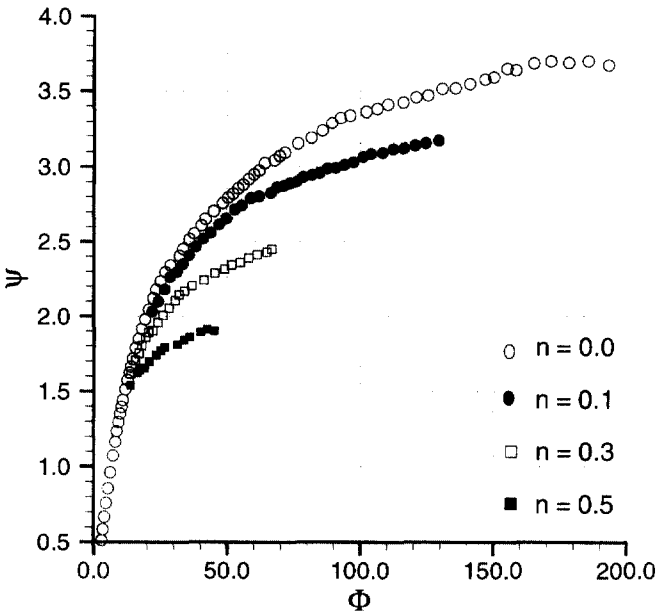

Fig. 8. Constraint factor calculated for the representative stress and strain values at the indentation edge using d_t.

indentation center, which depends on the friction between the indenter and the specimen, ε_{eq}^{pl} reaches a maximum and then decreases with a smaller gradient to the indentation center. This implies that by placing the point at which the stresses ad strains are related to the indentation parameters to some other location beneath the indenter, the σ_t–ε_p curve can be predicted for ε_p higher than 0.2. The new selected point can be called the "reference point". Stresses and strains at this point were related to the indentation parameters by a new set of equations, different from those established for the stress and strain values at the indentation edge.

In the present analysis, the reference point was selected at the maximum strain point, which is at the radius of about $d_t/3$ from the indentation center. A new relationship between ε_p and the indentation parameters was established for this point. It was written as a function of n to account for the piling-up or sinking-in effect:

$$\varepsilon_{p,max} = \left(0.5n + \frac{1.44}{\sqrt{n+0.1}} - 1.6\right)\left(\frac{d_t}{D}\right)^2. \tag{13}$$

The corresponding ψ value, ψ_{max}, shows the same behavior as that computed at the indentation edge using the actual contact diameter. After it reaches a certain value (i.e., total plastic state is reached), ψ_{max} remains constant and independent of Φ, $\psi_{max} = \psi^c_{max}$, but on the other hand, is an obvious function of n, because the indentation diameter d_t was used. Before the ψ_{max} curves reach their constant value ψ^c_{max}, they follow the same path, which happens to be a line in the ψ_{max} vs ln(Φ) plot (see Fig. 9), and could be approximated by a function [see eqn (14)], which is very similar to eqn (2). Perhaps, the same explanation about the transition regime, which is a combination of elastic and plastic deformation, where ψ is a linear function of ln(Φ), and the fully plastic regime, where the plastic deformation reaches the free material surface and ψ has a constant value ψ^c can be considered here. The form of the function is:

$$\psi_{max} = \begin{cases} -0.65 + \ln(\Phi) \\ \psi^c_{max} \end{cases} \tag{14}$$

The $\psi_{max} = -0.65 + \ln(\Phi)$ line should be followed until it reaches the ψ^c_{max} value pertinent

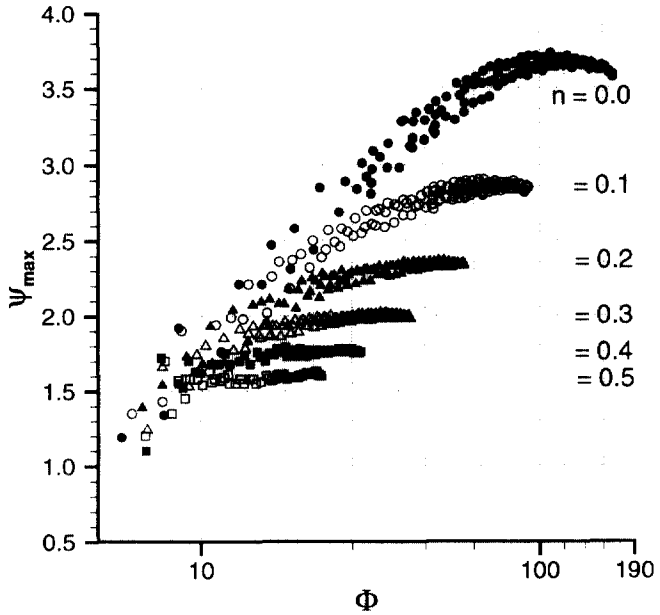

Fig. 9. Plot of ψ_{max} vs Φ for the maximum strain reference point.

to the current n value. Furthermore, ψ^c_{max} can be expressed as a function of n by the following equation:

$$\psi^c_{max} = -0.81 + \frac{2}{\sqrt{n+0.2}}. \tag{15}$$

Figure 9 shows the plot of ψ_{max} as a function of the parameter Φ.

3.3.3. *Minimum strain method.* In contrast to the approach presented in the previous section, we now look for the reference point that would give a reliable result up to the strain value of about 0.05. Placing the point at a distance of about $d_t/10$ outward the indentation edge, ε^{pl}_{eq} has the maximum value of 0.26 for $n = 0.0$. The correlation between ε^{pl}_{eq} and d_t/D at this point can be approximated by the following equation:

$$\varepsilon_{p,\min} = \left(-2 + 0.87n + \frac{1.47}{\sqrt{n+0.36}}\right)\left(\frac{d_t}{D}\right)^{2.45-0.85n} \tag{16}$$

The corresponding ψ_{min} vs Φ plot, calculated at the radial distance of $d_t/10$ from the indentation edge, can be derived in the same way as described earlier in the maximum strain approach. The results show that almost a constant ψ_{min} ($\psi_{min} = 3.75$) value can be accepted for $n < 0.3$.

ε^{pl}_{eq} at the observed point depends on n and d_t/D. The value of ε^{pl}_{eq} is higher ($0.12 < \varepsilon^{pl}_{eq} < 0.25$) for materials with low n ($n < 0.1$) and lower ($0.01 < \varepsilon^{pl}_{eq} < 0.03$) for materials with higher n ($n > 0.3$). A favorable ε^{pl}_{eq} range occurs at $n = 0.2$ where the ε^{pl}_{eq} reaches the value of 0.06 at $d_t/D = 0.75$. An efficient method would give results up to the desired strain value, independently of the n value. To achieve this, one can use the ε^{pl}_{eq}–d_t/D curve obtained for $n = 0.2$ for all n values. This means that the reference point moves to a different location for materials with n different than 0.2. The corresponding ψ_{min} curves can be approximated as:

$$\psi_{\min} = (3.65 - 4.30n^2 + 4.36n^3)\left(\frac{d_t}{D}\right)^{(-3.18n^2+2.89n^3)} \tag{17}$$

The above equations provide a good fit to the computed data. They are rather sensitive to n, which means that a good estimate of n is required. The equation for σ_t [eqn (1)] remains the same as was used for the Tabor's approach, except for the parameter ψ which changes to $\psi_{\max}$ for the maximum strain approach, and to $\psi_{\min}$ when the minimum strain approach is considered.

3.3.4. *Determining n from indentation data.* A strong n influence introduced in the above equations accounts for both, the difference between d_t and the actual contact diameter, and the direct effect of n on ψ. Using d_t of loaded indentations makes the procedure easier to use, because no intermediate unloading is required, and also more comparable, because of the unique way for determining the indentation diameter. A question arises at the point when one wants to apply the equations to an experimental procedure, because the equations are n dependent. Any approach to determine σ_t–ε_p curve by the indentation test requires information of the indentation diameter. Since the piling-up or sinking-in phenomena considerably influence the indentation diameter, and the phenomena depends on n, it is obvious that the knowledge of n is mandatory. Therefore, it is essential to extract that information from the indentation F–h measurement results. Several possibilities are discussed below:

1. Considering Meyer's law, $F = kd^m$, and the fact that $n = m-2$, one can estimate n from the measured F–d data. It turns out that the method works well and that n can be determined with reasonable accuracy for a broad range of materials. The difficulty of this approach is that the information of the actual contact diameter, d, is required, and, our analysis shows that n obtained using this approach, while substituting d with d_t of a loaded or unloaded indentation, does not always give accurate results (see also Field and Swain, 1995).
2. The loading part of the F–h curve can provide additional information (Taljat, 1996). A relationship among loading slope, σ_y, and n, proposed by Taljat (1996) can be solved if one has information of σ_y, in addition to the measured value of loading F–h slope.

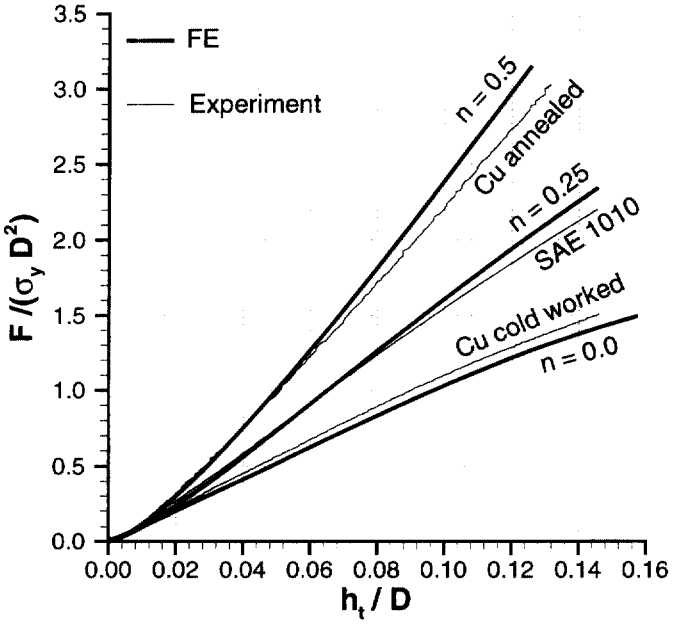

Fig. 10. Loading $F/\sigma_y D^2$–h_t/D curve shape as a function of n.

3. Another possibility is the shape of the loading F–h curve. Results from the FE analyses and experimental work suggest that the relationship between F and h is almost linear (except the first part) due to the combination of two inverse nonlinearities (nonlinear indenter geometry and nonlinear material characteristic). The linear relationship is usually obtained at a certain d/D range ($0.1 < d/D < 0.7$). After the indenter is pushed to more than a certain depth, the F–h plot becomes nonlinear and curved toward the h axis. The explanation for this phenomenon could be the effect of material saturation, which occurs after a critical amount of deformation is exceeded, or also, the nonlinearity effect of the sphere geometry compared to the effect of material nonlinear characteristic is becoming weaker as the penetration depth increases beyond a certain limit. It was observed that the portion of F–h loading curve which is expected to be linear is slightly curved toward the F axis for materials with high n and curved toward the h axis for materials with low n (see Fig. 10).
4. Combining the observed phenomenon with the method of measuring piling-up or sinking-in of the material around the impression should give a reasonably good estimate of the strain-hardening exponent, providing the E/σ_y value of the material tested is known [see Fig.4, Fig.5, and eqns (9) to (12)].

4. EXPERIMENTAL RESULTS AND METHOD VERIFICATION

Experimental work has been performed using an instrumented spherical-indentation testing system. The technique is based on displacement and/or load-controlled indentation by a spherical indenter. The experimental system includes: (1) a two-column frame with electromechanically driven testing head, indenter, linear variable differential transformer sensor, and load cell; (2) a data acquisition system, control unit, and driver for the servo motor; and (3) a personal computer with specially developed software needed to operate the system.

Several tests were performed on pressure vessel steel A533-B steel, carbon steel SAE1010, cold-worked copper, annealed copper, and Al–Mg alloy. Tests were performed using a 1.576 mm diameter tungsten carbide spherical indenter. Indentation F–h data were continuously measured and recorded during the experiment. Also, compression tests were carried out on the same material in order to verify the new method for determining σ_t–ε_p curve.

The continuous loading F–h data were considered for calculation of the σ_t–ε_p curve by the new approach. σ_t was calculated by eqn (1) using the appropriate value of ψ; $\psi_{\min}$ for the minimum strain approach and $\psi_{\max}$ for the maximum strain approach, and using d_t for calculating P_m. ε_p was calculated by $\varepsilon_{p,\min}$ for the minimum strain approach and $\varepsilon_{p,\max}$ for the maximum strain approach.

Figures 11(a)–(d) show the comparison between compression tests and new method for cold-worked copper, A533-B steel, Al–Mg alloy, and annealed copper. In general the σ_t–ε_p curves obtained by the method proposed agree well with the compression σ_t–ε_p curves. The agreement is excellent for A533-B, having the same E/σ_y ratio as the one used for the method development. The initial part of the predicted σ_t–ε_p curve for cold-worked copper does not agree well with the compression σ_t–ε_p curve, because of the sharp transition from elastic to plastic behavior, whereas the prediction at higher strains is good. The predicted σ_t–ε_p curve underestimates the initial part of the Al–Mg compression σ_t–ε_p curve by approximately 10%, and it overestimates the compression σ_t–ε_p curve of annealed copper.

5. CONCLUSIONS

The FE analysis of the spherical indentation was performed using ABAQUS FE code. The FE load-depth results were compared with the experimental results and a good agreement was obtained. A series of FE calculations was carried out for materials with various properties. The stress–strain field in the material beneath the indenter was analyzed, and Tabor's equation for calculating ε_p from the indentation data was verified.

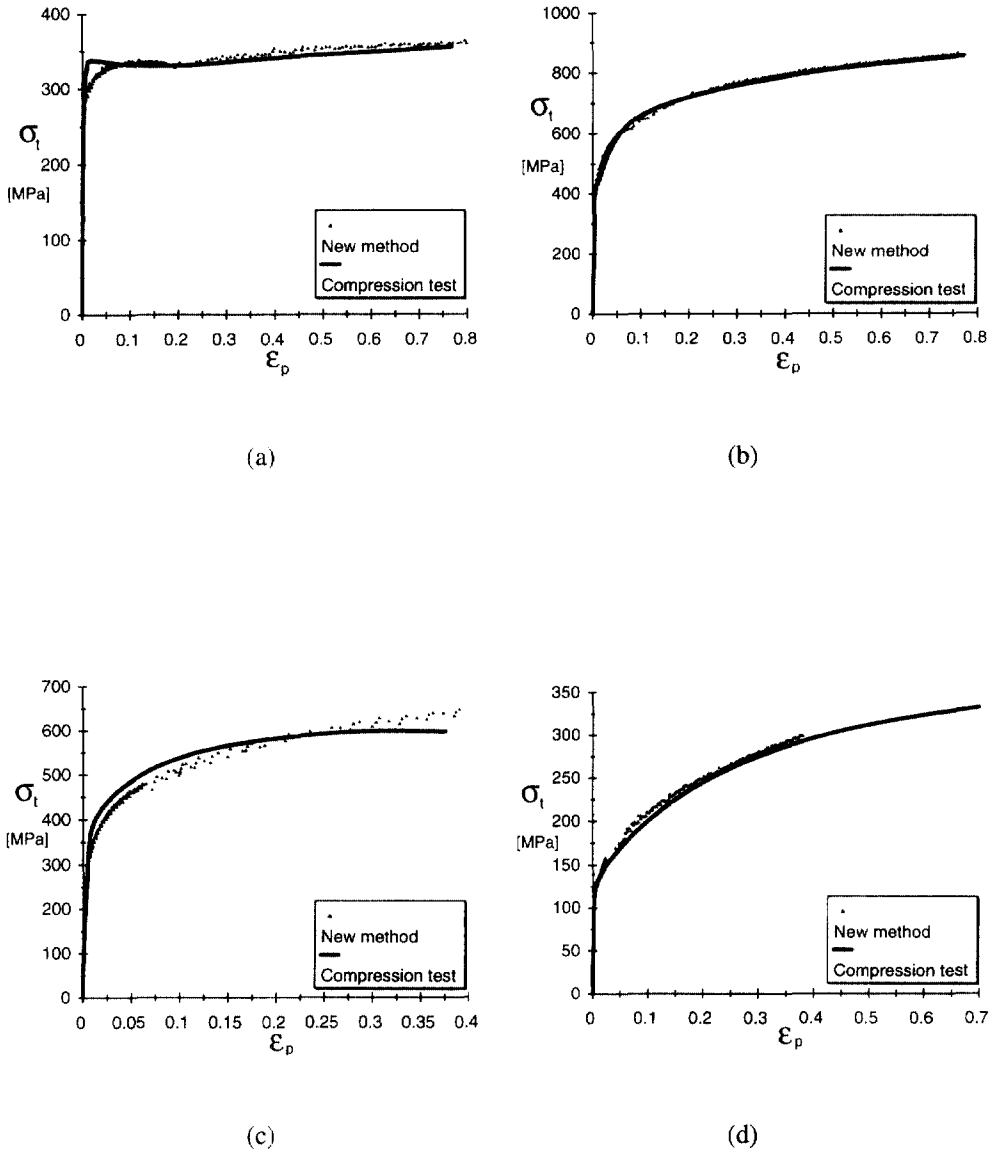

Fig. 11. Comparison between compression and indentation σ_t–ε_p curve: (a) cold-worked copper; (b) A533-B steel; (c) Al–Mg alloy; (d) annealed copper.

The importance of an accurate measure of the actual indentation contact diameter was discussed and different equations for its prediction were evaluated in terms of their effect on the subsequent procedure for the stress–strain curve calculation. Also, the effect of piling-up and sinking-in on the actual contact diameter was evaluated.

Equations for calculating the material σ_t–ε_p curve from the indentation parameters [see eqns (1) and (4)] relate the indentation parameters to the material stress–strain state at the indentation edge. The maximum ε_p value calculated from eqn (4) is 0.2. By moving the point for which the σ_t–ε_p relation is established, i.e., "the reference point," to a region of maximum strain (approximately to a radius of $d_t/3$ from the indentation center), the material σ_t–ε_p curve can be predicted at much higher strains (ε_p up to 1.6). On the other hand, by moving the reference point outward from the indentation edge, the material σ_t–ε_p curve can be predicted for lower strains (yield strain $< \varepsilon_p < 0.1$). New relationships for ε_p and ψ were proposed which enable continuous σ_t–ε_p curve calculation during the loading process (no intermediate unloading is required) by the mentioned maximum and minimum strain approaches. This was accomplished by using an apparent indention diameter, defined

with the intersection of the indenter surface and the undeformed material surface, in the σ_i–ε_p curve calculation.

The proposed equations are written as functions of n, which also takes into account the difference between the apparent indentation diameter used in the calculation and the actual contact diameter. Therefore, n should be measured during the indentation process in order to calculate the σ_i–ε_p curve. Some methods for determining n from the indentation data were evaluated. It was observed that the shape of the loading F–h curve correlates with n.

Acknowledgments—The authors would like to thank Prof. George M. Pharr and Dr Gorti Sarma for reviewing the paper. The research was sponsored in part by an appointment to the Oak Ridge National Laboratory Postdoctoral Research Associates Program administered jointly by the Oak Ridge Institute for Science and Education and Oak Ridge National Laboratory. The research was also sponsored by the Division of Materials Science, U.S. Department of Energy, under contract De-AC05-96OR22464 with Lockheed Martin Energy Research Corp., and by the U.S. Navy, Office of Naval Research under interagency agreement DOE No. 1866-E126-A1, Navy No. N000014-92-F-0063 under U.S. Department of Energy contract De-AC05-96OR22464 with Lockheed Martin Energy Research Corp.

REFERENCES

ABAQUS (1996), Users' Manual, Version 5.5. Hibbitt, Karlsson & Sorensen.

Au, P., Lucas, G. E., Scheckerd, J. W. and Odette, G. R. (1980) Flow property measurements from instrumented hardness tests. In *Nondestructive Evaluation in the Nuclear Industry*, pp. 579–610, ASM International, Metals Park, OH.

Bolshakov, A., Oliver, W. C. and Pharr, G. M. (1996) Finite element studies of the influence of pile-up on the analysis of nanoindentation data, accepted for publication in *Thin Films: Stresses and Mechanical Properties VI*—Materials Research Society Symposium Proceedings, **436**, ed. W. W. Gerberich, H. Gao, J. E. Sundgren and S. P. Baker, Materials Research Society, Pittsburgh, PA.

Field, J. S. and Swain, M. V. (1995) Determining the mechanical properties of small volumes of material from submicrometer spherical indentations. *J. Mater. Res.* **10**(1), 101–112.

Francis, H. A. (1976) Phenomenological analysis of plastic spherical indentation, *Trans. ASME, J. En. Mater. Technol.* 272–281.

George, R. A., Dinda, S. and Kasper, A. S. (1976) Estimating yield strength from hardness test. *Met Progress*, 30–35.

Hertz, H. (1986) *Miscellaneous Papers by H. Hertz*, ed. Jones and Schott, Macmillan, London.

Hill, R., Storakers, B. and Zdunek, A. B. (1989) A theoretical study of the brinell hardness test. *Proc. R. Soc. London* **A423**, 301.

Johnson, K. L. (1970) The correlation of indentation experiments. *J. Mech. Phys. Solids* **18**, 115–126.

Matthews, J. R. (1980) Indentation hardness and hot pressing. *Acta Metall.* **28**, 311–318.

Norbury, A. L. and Samuel, T. (1928) The recovery and sinking-in or piling-up of material in the brinell test, and the effects of these factors on the correlation of the brinell with certain other hardness tests. *J. Iron. Steel Inst.* **117**, 673.

Sinclair, G. B., Follansbee, P. S. and Johnson, K. L. (1985) Quasi-static normal indentation of an elasto-plastic half-space by a rigid sphere—II. results. *Int. J. Solids Structures.* **21**(8), 865–888.

Tabor, D. (1951) *The Hardness of Metals*. Clarendon Press, Oxford.

Taljat, B. (1996) *Determining Stress–Strain Curves of Metals by Nondestructive Continuous Ball-Indentation Methods*. Ph.D. Thesis, University of Ljubljana, Slovenia.

Taljat, B., Zacharia, T., and Haggag, F. M. (1997) Analysis of ball-indentation load-depth data: part I—determining elastic modulus. *J. Mater. Res.* **12**(4), 965–974.

Tirupatahiah, Y. (1991) On the constraint factor associated with the indentation of work-hardening materials with a spherical ball. *Metall. Trans. A.* **22A**, 2375–2384.